metals

MDPI

Article

The Impact of the Composition Effect on Ferromagnetic Properties of Tb_2Co_2Ga

Seiya Tanaka [1], Hirotaka Terada [1], Naoki Shirakawa [2], Masami Tsubota [3] and Jiro Kitagawa [1,*]

1 Department of Electrical Engineering, Faculty of Engineering, Fukuoka Institute of Technology, 3-30-1 Wajiro-higashi, Higashi-ku, Fukuoka 811-0295, Japan; s1552026@bene.fit.ac.jp (S.T.); s1452006@bene.fit.ac.jp (H.T.)

2 Flexible Electronics Research Center, National Institute of Advanced Industrial Science and Technology, Tsukuba, Ibaraki 305-8565, Japan; shirakawa.n@aist.go.jp

3 Physonit Inc., 6–10 Minami-Horikawa, Kaita Aki, Hiroshima 736-0044, Japan; tsubota@physonit.jp

* Correspondence: j-kitagawa@fit.ac.jp

Received: 18 October 2019; Accepted: 19 November 2019; Published: 20 November 2019

Abstract: The ferromagnetic properties of Tb_2Co_2Ga, crystallizing into an orthorhombic W_2CoB_2-type structure, were investigated by preparing 11 polycrystalline samples with different starting atomic compositions. We found that Tb_2Co_2Ga possesses a homogeneity range in the ternary phase diagram. The Curie temperature T_C is sensitive to the atomic composition and ranges rather widely, i.e., from 75 to 145 K. For the samples with a T_C above 90 K, the nearest Tb–Tb and the Tb–Co distances would be important factors deciding T_C, considering the RKKY interaction through the hybridization between Tb and Co atoms. An anisotropic change of two kinds of Co–Tb–Co angles in the octahedron formed by two Tb and four Co atoms occurs in the samples with a T_C lower than 90 K. Such a change of octahedral parameters seems to be related to a difference of shapes in the ac magnetization anomaly at T_C between the samples in the lowest T_C (~ 75 K) group and those in the other groups.

Keywords: ferromagnetism; W_2CoB_2-type structure; composition effect; magnetic measurements; lattice parameters

1. Introduction

Several ferromagnetic compounds of R_2Co_2Al and R_2Co_2Ga (R = heavy rare earth) with an orthorhombic W_2CoB_2 (Mo_2NiB_2) -type structure [1] are attractive as magnetic refrigeration materials [2–5]. Recently, we studied the orthorhombic W_3CoB_3-type Tb_3Co_3Ga that is located near Tb_2Co_2Ga in the ternary phase diagram [6]. A polycrystalline Tb_3Co_3Ga sample also showed ferromagnetism, but the Curie temperature T_C ranged from 90 K to 117 K, depending on the starting atomic composition. The actual atomic composition that correlates with the starting composition has revealed the existence of a homogeneity range, especially along the Ga concentration. The crystal structure parameters, which slightly change with the atomic composition, severely affect T_C.

It has been recently reported [7] that Tb_2Co_2Ga is a ferromagnet with T_C = 86 K. Figure 1a,b shows the crystal structure of Tb_2Co_2Ga. In the orthorhombic structure, with the space group of Immm (No.71), Tb, Co, and Ga atoms occupy the crystallographic 4h, 4f, and 2a sites, respectively. Two Tb and the nearest neighboring four Co atoms build an octahedron, the arrangement of which can be regarded as a rectangular lattice in the *a*-*b* plane (see Figure 1b). The rectangular lattice stacks along the *c*-axis. The isostructural Tb_2Co_2Al has been reported to be a ferromagnet [4] below 111 K. A neutron diffraction study [4] has clarified that Tb and Co sublattices form a *c*-axis ferrimagnetic ordering. The magnetic moment of Tb at 2 K is 8.86 μ_B, which dominates over that of Co with 0.26 μ_B.

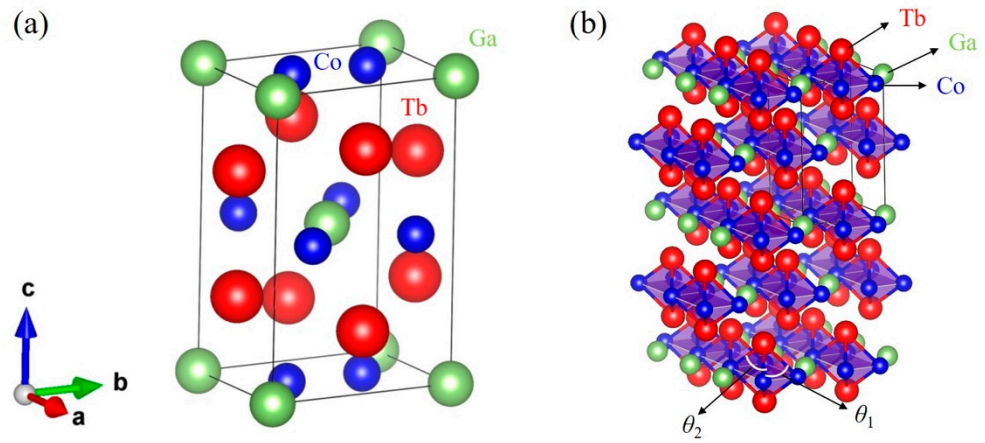

Figure 1. (**a**) Unit cell of Tb_2Co_2Ga. (**b**) Crystal structure of Tb_2Co_2Ga, emphasizing the polyhedral arrangement. The solid line represents the unit cell. θ_1 and θ_2 are Co–Tb–Co angles in the octahedron formed by two Tb atoms and the nearest neighboring four Co atoms.

As in the case of Tb_3Co_3Ga, we can expect a composition effect for Tb_2Co_2Ga. If a homogeneity range exists in a metallurgical phase diagram, the magnetic ordering temperature often varies depending on the atomic composition. Such a composition effect is actually observed [8] in $Nd_3Pd_{20}Ge_6$, which shows a slight decrease of the Néel temperature as the Pd atomic composition is increased from 19.2 to 21. Another example is $Mn_{1+x}Ga$, which is a ferromagnet showing a reduced T_C with decreasing Mn concentration [9]. The study that found this effect presented a detailed composition effect of ferromagnetic properties that depend on the crystal structure parameters.

If Tb_2Co_2Ga shows a composition effect based on ferromagnetic properties, the effect would depend on the crystal structure parameters, which may play a crucial role in the design of magnetic refrigeration materials with a W_2CoB_2 -type structure. Therefore, it is important to know the relationships between the crystal structure parameters and ferromagnetic properties in W_2CoB_2 -type compounds; however, this has not been well explored. In this paper, we report the composition effect of the magnetic properties of polycrystalline Tb_2Co_2Ga by a metallographic examination and measurement of the magnetic susceptibility and the magnetization curve.

2. Materials and Methods

Eleven polycrystalline samples, A to K, with different starting atomic compositions, as listed in Table 1, were synthesized by a home-made arc furnace. The constituent elements of Tb (Nippon Yttrium, Omuta, Japan, bulk, 99.9%), Co (Kojundo Chemical Laboratory, Sakado, Japan, bulk, 99.9%) and Ga (Kojundo Chemical Laboratory, Sakado, Japan, bulk, 99.99%), placed on a water-cooled Cu hearth, were arc-melted in an Ar atmosphere. Each as-cast sample was sealed in an evacuated quartz tube, which was heated to 650 °C and held at that temperature for 4 days. In Table 1, all the samples are labeled into four groups (G1, G2, G3, and G4) based on the value of T_C, and the samples in the G4 group are further divided into three subgroups (SG4-1, SG4-2 and SG4-3), as explained below. The starting atomic composition covers Tb: 39–45%, Co: 36–42% and Ga: 17–24%. The location of each sample, with its starting atomic composition, is depicted in the Tb–Co–Ga ternary phase diagram (see Figure 2a), in which the impurity phases detected in this study are also marked.

Table 1. Starting atomic compositions and determined compositions of the main phase by EDX measurement for prepared samples.

Group	Subgroup	Sample	Starting Composition	Tb_2Co_2Ga Main Phase
G1	-	A	$Tb_{41.7}Co_{41.7}Ga_{16.6}$	$Tb_{40.1(6)}Co_{39.8(8)}Ga_{20.1(4)}$
G1	-	B	$Tb_{45.0}Co_{38.0}Ga_{17.0}$	$Tb_{39.9(8)}Co_{40.7(4)}Ga_{19.4(9)}$
G2	-	C	$Tb_{41.4}Co_{39.4}Ga_{19.2}$	$Tb_{39.9(3)}Co_{39.4(2)}Ga_{20.6(5)}$
G2	-	D	$Tb_{43.9}Co_{36.8}Ga_{19.3}$	$Tb_{40.3(8)}Co_{38.8(9)}Ga_{21.0(2)}$
G3	-	E	$Tb_{42.0}Co_{38.0}Ga_{20.0}$	$Tb_{39.7(8)}Co_{38.6(7)}Ga_{21.7(5)}$
G3	-	F	$Tb_{42.9}Co_{35.7}Ga_{21.4}$	$Tb_{39.8(6)}Co_{39.7(5)}Ga_{21.5(4)}$
G4	SG4-1	G	$Tb_{41.0}Co_{37.0}Ga_{22.0}$	$Tb_{39.6(7)}Co_{37.7(9)}Ga_{22.7(6)}$
G4	SG4-1	H	$Tb_{40.6}Co_{38.7}Ga_{20.7}$	$Tb_{39.5(4)}Co_{38.5(9)}Ga_{22.1(8)}$
G4	SG4-2	I	$Tb_{40.0}Co_{40.0}Ga_{20.0}$	$Tb_{39.4(5)}Co_{37.7(6)}Ga_{22.9(9)}$
G4	SG4-3	J	$Tb_{38.9}Co_{37.0}Ga_{24.1}$	$Tb_{39.1(1)}Co_{38.4(6)}Ga_{22.5(8)}$, $Tb_{40.9(6)}Co_{38.5(6)}Ga_{20.6(9)}$
G4	SG4-3	K	$Tb_{39.0}Co_{39.0}Ga_{22.0}$	$Tb_{39.1(3)}Co_{38.0(4)}Ga_{22.9(2)}$

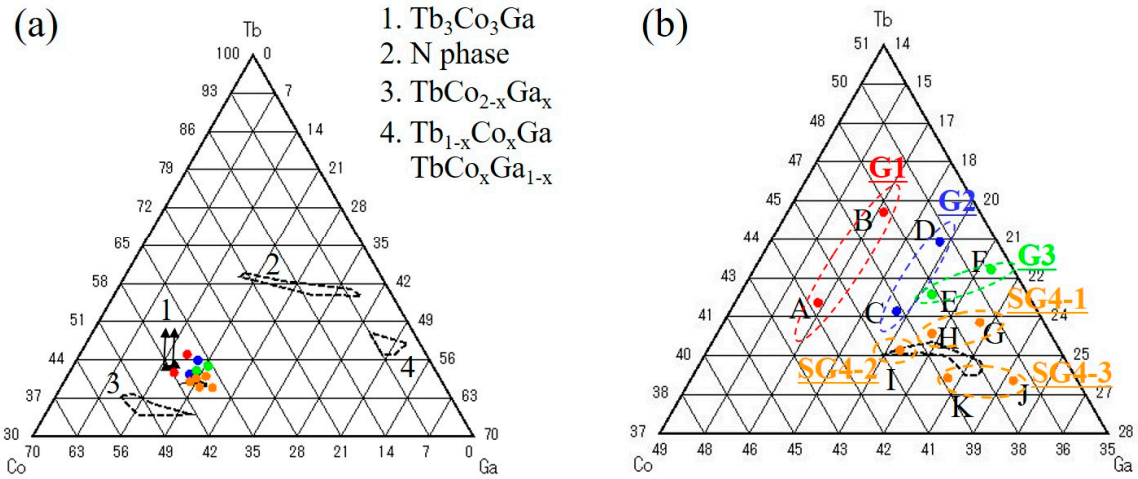

Figure 2. (**a**) Ternary phase diagram of the Tb–Co–Ga system for prepared samples plotted based on their starting compositions (filled colored circles). The impurity phases (Tb_3Co_3Ga, the N phase, $TbCo_{2-x}Ga_x$, $Tb_{1-x}Co_xGa$ and $TbCo_xGa_{1-x}$) are also added. The area surrounded by broken lines indicates a range of the solid solution detected by EDX measurement. The homogeneity range of Tb_3Co_3Ga is depicted by the black triangles. (**b**) Expanded diagram around the Tb_2Co_2Ga phase. The area surrounded by black broken-lines indicates a range of the solid solution of Tb_2Co_2Ga detected by EDX measurement.

X-ray diffraction patterns were recorded by using a powder X-ray diffractometer (XRD-7000L Shimadzu, Kyoto, Japan,) with Cu-Kα radiation. The 2θ range was between 10° and 90°. The microstructure of the prepared sample was checked by a field emission scanning electron microscope (JSM-7100F FE-SEM; JEOL, Akishima, Japan,), and the atomic composition in each area of the sample was determined by an energy dispersive X-ray (EDX) spectrometer attached to the FE-SEM.

The temperature dependence of ac magnetic susceptibility χ_{ac} (T) between 3 K and 300 K was measured by a home-made system in a closed-cycle He gas cryostat. The amplitude and frequency of the ac field were 5 Oe and 800 Hz, respectively. The temperature dependence of dc magnetic susceptibility χ_{dc} (T) between 5 K and 300 K, and the magnetization curves were measured by a MPMS magnetometer (Quantum Design, San Diego, CA, USA).

3. Results and Discussion

3.1. XRD Pattern and Microstructure

The X-ray diffraction (XRD) patterns of all samples are shown in Figure 3, which also includes the simulated pattern of Tb_2Co_2Ga. Each pattern of the main phase matches with that of Tb_2Co_2Ga, while obvious impurity peaks appear in the samples H to K. The impurity phases are discussed in the results of EDX measurement. From samples A to K, each peak position shifts, indicating a change of lattice parameters and the existence of a homogeneity range. The composition dependences of the crystal structure parameters are explained after showing the results of metallographic examinations.

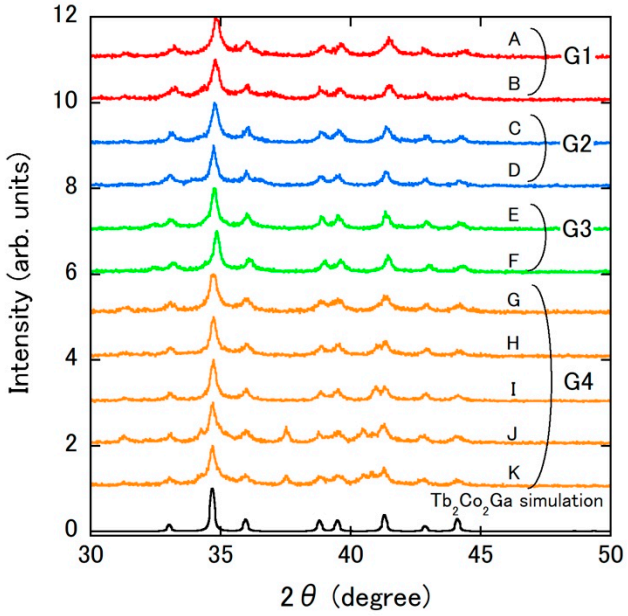

Figure 3. XRD patterns of prepared samples. The simulated pattern of Tb_2Co_2Ga with a = 4.103 Å, b = 5.421 Å and c = 8.433 Å is also shown. The origin of each pattern is shifted by an integer value.

Back-scattered electron images obtained by FE-SEM with electron beams of 15 keV are shown in Figure 4a–f for the samples A to F, and in Figure 5a–e for samples G to K, respectively. The atomic compositions obtained by EDX measurement of all the samples are listed in Tables 1 and 2. The number of data collection points per sample is 10. The composition of the main phase for each sample is close to Tb_2Co_2Ga. In the samples A to C, the compositions of the Tb_2Co_2Ga phases are almost stoichiometric. Going on to samples C to K, a gradual replacement of Tb and Co atoms by Ga atom is observed (see Table 1). Thus, Tb_2Co_2Ga possesses a homogeneity range as indicated by black broken lines in Figure 2b. In this study, the homogeneity range is defined as the composition range detected by EDX for a target compound. The samples A and B contain a small amount of Tb_3Co_3Ga phase, located near these samples in the ternary phase diagram (see Figure 2a). When the Ga concentration of the Tb_2Co_2Ga phase is below 21.7%, it is accompanied by the N phase (see Tables 1 and 2), the amount of which is rather large in samples B and D (see Figure 4b,d). This is consistent with the phase relation displayed in Figure 2b. The pseudo binary $TbCo_{2-x}Ga_x$ appears in samples A, C, G, H, I, and K, which are located near $TbCo_{2-x}Ga_x$ (see Figure 2a). Because the locations of samples G to K are rather far away from that of the N phase, these samples do not contain the N phase; however, another impurity phase is detected, shown as small bright areas in Figure 5a–e. The impurity phase is presumably $Tb_{1-x}Co_xGa$ for the samples G, H, I, and K, or $TbCo_xGa_{1-x}$ for sample J. In sample J, the Tb_2Co_2Ga phase seems to be inhomogeneous, which is deduced by the observation of two phases with slightly different atomic compositions, and the χ_{ac} (T) results, as mentioned below.

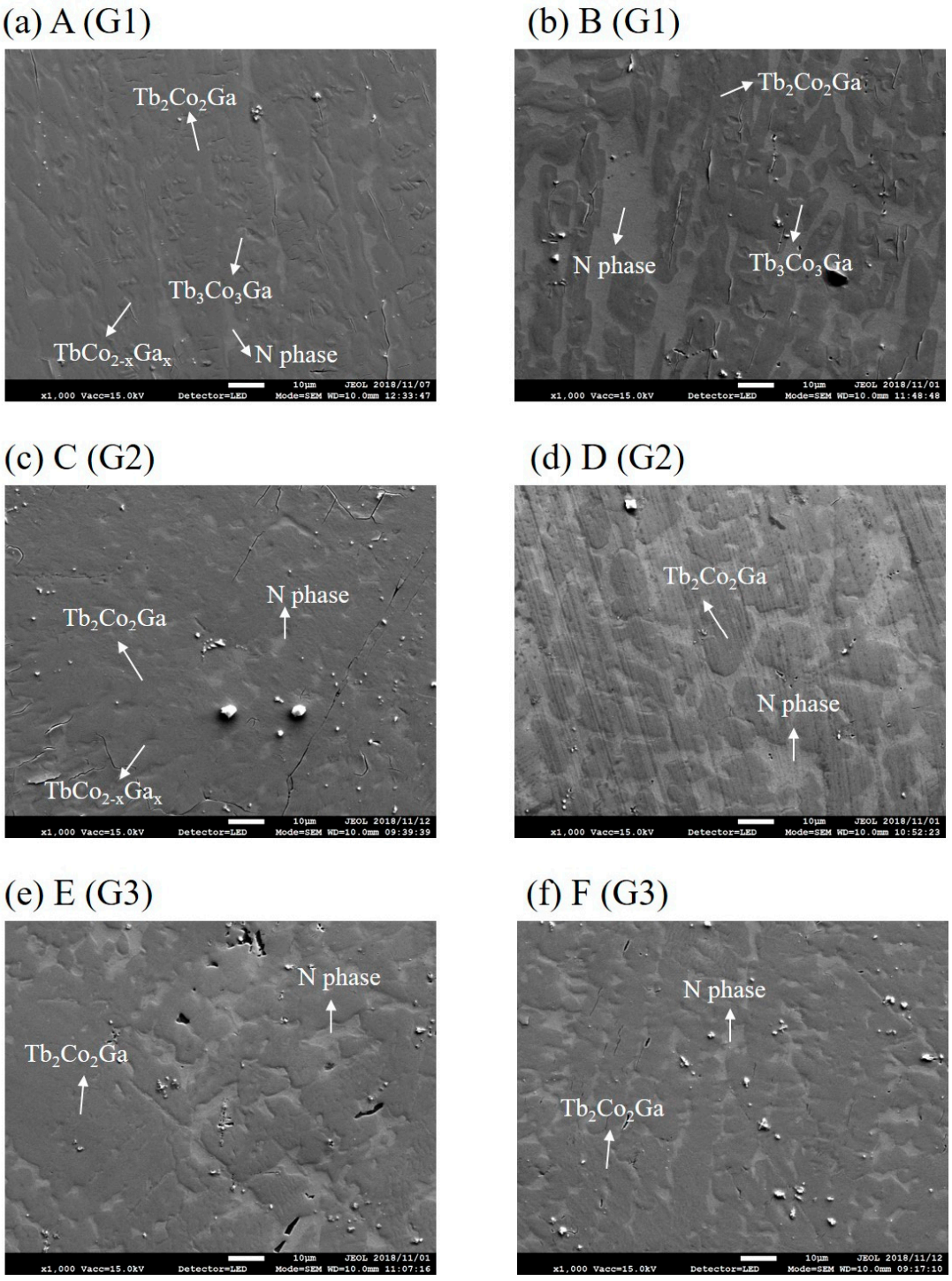

Figure 4. Back-scattered electron (15 keV) images of samples (**a**) A, (**b**) B, (**c**) C, (**d**) D, (**e**) E, and (**f**) F, respectively.

The lattice parameters of all samples were obtained by the least square method with the help of RIETAN-FP program [10,11] using the XRD patterns listed in Table 3. The actual fitting range of 2θ was between 10° and 90°, in which impurity phases with known crystal structures are also considered, but diffraction peaks originating from impurity phases with unknown structures are eliminated. Focusing on the Ga-concentration dependence of the obtained lattice parameters, it can be said that *a* increases with the increase of Ga concentration (see also Figure 9a). On the other hand, *b* (*c*) monotonously increases (decreases) from sample A to F (in the G1, G2 and G3 groups); the sample dependence is

not so straightforward in the G4 group. Samples G to I show the slight contraction of *b* compared to sample F, but the opposite behavior is observed in samples J and K. Compared to *c* of sample F, *c*'s of samples G and H are decreased, although samples I, J, and K show an increase of *c*.

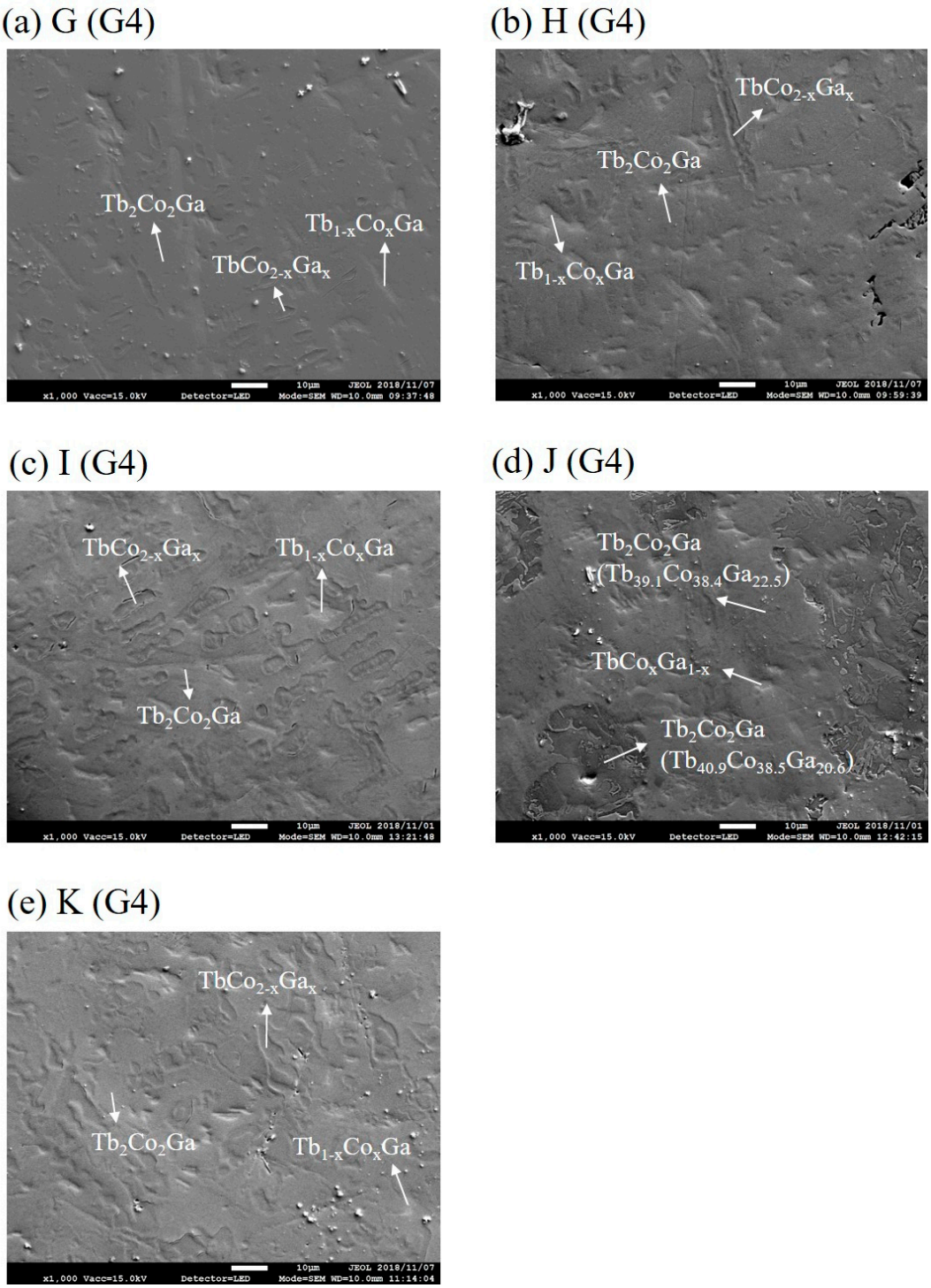

Figure 5. Back-scattered electron (15 keV) images of samples (**a**) G, (**b**) H, (**c**) I, (**d**) J, and (**e**) K, respectively.

Table 2. Atomic compositions of impurity phases determined by EDX measurement for prepared samples.

Group	Subgroup	Sample	Tb_3Co_3Ga	N phase	$TbCo_{2-x}Ga_x$	$Tb_{1-x}Co_xGa$ (G,H,I,K) or $TbCo_xGa_{1-x}$ (J)
G1	-	A	$Tb_{42.6(4)}Co_{42.5(1)}Ga_{14.9(3)}$	$Tb_{59.2(6)}Co_{22.5(7)}Ga_{18.3(3)}$	$Tb_{37.3(8)}Co_{52.4(9)}Ga_{10.3(9)}$	-
G1	-	B	$Tb_{43.1(2)}Co_{40.9(5)}Ga_{16.0(7)}$	$Tb_{59.9(6)}Co_{21.4(8)}Ga_{18.8(6)}$	-	-
G2	-	C	-	$Tb_{56(1)}Co_{13(1)}Ga_{31(1)}$	$Tb_{38(1)}Co_{50(1)}Ga_{12(1)}$	-
G2	-	D	-	$Tb_{58.4(8)}Co_{15.8(8)}Ga_{25.8(3)}$	-	-
G3	-	E	-	$Tb_{57(1)}Co_{6(2)}Ga_{36.8(8)}$	-	-
G3	-	F	-	$Tb_{55.7(8)}Co_{5(1)}Ga_{39.3(9)}$	-	-
G4	SG4-1	G	-	-	$Tb_{33.8(8)}Co_{50.8(9)}Ga_{15.4(3)}$	$Tb_{45.6(3)}Co_{4.2(8)}Ga_{50.3(3)}$
G4	SG4-1	H	-	-	$Tb_{36(1)}Co_{48(1)}Ga_{16(1)}$	$Tb_{45(1)}Co_{5(1)}Ga_{49(1)}$
G4	SG4-2	I	-	-	$Tb_{34.0(5)}Co_{51.4(8)}Ga_{14.5(5)}$	$Tb_{44.9(3)}Co_{7(2)}Ga_{48(2)}$
G4	SG4-3	J	-	-	-	$Tb_{49(1)}Co_{7(2)}Ga_{43(1)}$
G4	SG4-3	K	-	-	$Tb_{34.0(5)}Co_{42.8(9)}Ga_{23.2(5)}$	$Tb_{47(1)}Co_{2.0(9)}Ga_{50(1)}$

Table 3. Atomic composition, lattice parameters, cell volume V, T_C determined by χ_{ac}, μ_{eff} and Θ of each Tb_2Co_2Ga sample.

Group	Subgroup	Sample	Composition of Tb_2Co_2Ga	a (Å)	b (Å)	c (Å)	V (Å^3)	T_C (K)	μ_{eff} (μ_B/Tb)	Θ (K)
G1	-	A	$Tb_{40.1(6)}Co_{39.8(8)}Ga_{20.1(4)}$	4.0889 (7)	5.407 (1)	8.448 (2)	186.8 (1)	146	7.70	190
G1	-	B	$Tb_{39.9(8)}Co_{40.7(4)}Ga_{19.4(9)}$	4.0882 (7)	5.405 (1)	8.451 (2)	186.7 (1)	145		
G2	-	C	$Tb_{39.9(3)}Co_{39.4(2)}Ga_{20.6(5)}$	4.0952 (5)	5.4182 (9)	8.436 (1)	187.18 (8)	101	9.83	98
G2	-	D	$Tb_{40.3(8)}Co_{38.8(9)}Ga_{21.0(2)}$	4.0955 (6)	5.4196 (9)	8.435 (1)	187.22 (9)	102		
G3	-	E	$Tb_{39.7(8)}Co_{38.6(7)}Ga_{21.7(5)}$	4.0969 (5)	5.4204 (8)	8.430 (1)	187.21 (8)	92		
G3	-	F	$Tb_{39.8(6)}Co_{39.7(5)}Ga_{21.5(4)}$	4.0983 (5)	5.4230 (7)	8.427 (1)	187.28 (7)	90	10.6	45
G4	SG4-1	G	$Tb_{39.6(7)}Co_{37.7(9)}Ga_{22.7(6)}$	4.0976 (7)	5.418 (1)	8.423 (2)	187.0 (1)	78	10.1	90
G4	SG4-1	H	$Tb_{39.5(4)}Co_{38.5(9)}Ga_{22.1(8)}$	4.0983 (6)	5.4189 (9)	8.424 (1)	187.08 (9)	75		
G4	SG4-2	I	$Tb_{39.4(5)}Co_{37.7(6)}Ga_{22.9(9)}$	4.1026 (5)	5.4211 (7)	8.433 (1)	187.56 (7)	76		
G4	SG4-3	J	$Tb_{39.1(1)}Co_{38.4(6)}Ga_{22.5(8)}$	4.1046 (7)	5.425 (1)	8.437 (2)	187.9 (1)	76		
G4	SG4-3	K	$Tb_{39.1(3)}Co_{38.0(4)}Ga_{22.9(2)}$	4.1037 (7)	5.425 (1)	8.443 (2)	188.0 (1)	71		

3.2. Magnetic Properties

Figure 6a–d show the χ_{ac} (T) of all samples, categorized by the T_C of the Tb_2Co_2Ga phase, indicated by arrows. The ferromagnetic states of several samples were checked by magnetization curves, as mentioned below. As in other ferromagnetic compounds [12,13], the peak position of χ_{ac} (T) is employed as T_C, which would be systematically governed by the atomic composition (see also Table 3). In the inset of Figure 6a, the χ_{ac} (T) of the sample with the starting composition $Tb_{42.9}Co_{50}Ga_{7.1}$ is exhibited. This sample contains the pseudo binary $TbCo_{2-x}Ga_x$ alloy and the N phase [6]. Two pronounced peaks are observed at approximately 250 and 60 K, for which the pseudo binary $TbCo_{2-x}Ga_x$ alloy and the N phase are responsible, respectively [6]. The x value of $TbCo_{2-x}Ga_x$ is estimated to be 0.22, corresponding to that of $TbCo_{2-x}Ga_x$ exhibiting ferromagnetic transitions at approximately 260 K [12]. The χ_{ac} peaks of sample A at approximately 260 K and 55 K can also be ascribed to the parasitic phases of $TbCo_{2-x}Ga_x$ and the N phase, respectively. Another small hump at approximately 90 K is due to the impurity phase of Tb_3Co_3Ga. These assignments are supported by the metallographic examination combined with the EDX measurement of sample A (see Tables 1 and 2). In sample B, the χ_{ac} peak at 55 K evolves in accordance with the increased area of the N phase observed by the FE-SEM image. The T_C intrinsic to the Tb_2Co_2Ga phase is approximately 145 K for each sample. As shown in Figure 6b, sample C shows almost a single peak at 101 K. The small amount of N phase detected by EDX is responsible for a small hump at 60 K. The enlarged N phase in sample D leads to an obvious χ_{ac} peak at 60 K, in addition to the ferromagnetic transition due to the Tb_2Co_2Ga phase at 102 K. In samples E and F (see Figure 6c), the T_C of the Tb_2Co_2Ga phase is further reduced to approximately 90 K, and a small anomaly due to the N phase is observed in sample E. In sample F, an χ_{ac} anomaly due to the N phase might be masked by a large χ_{ac} peak at 90 K.

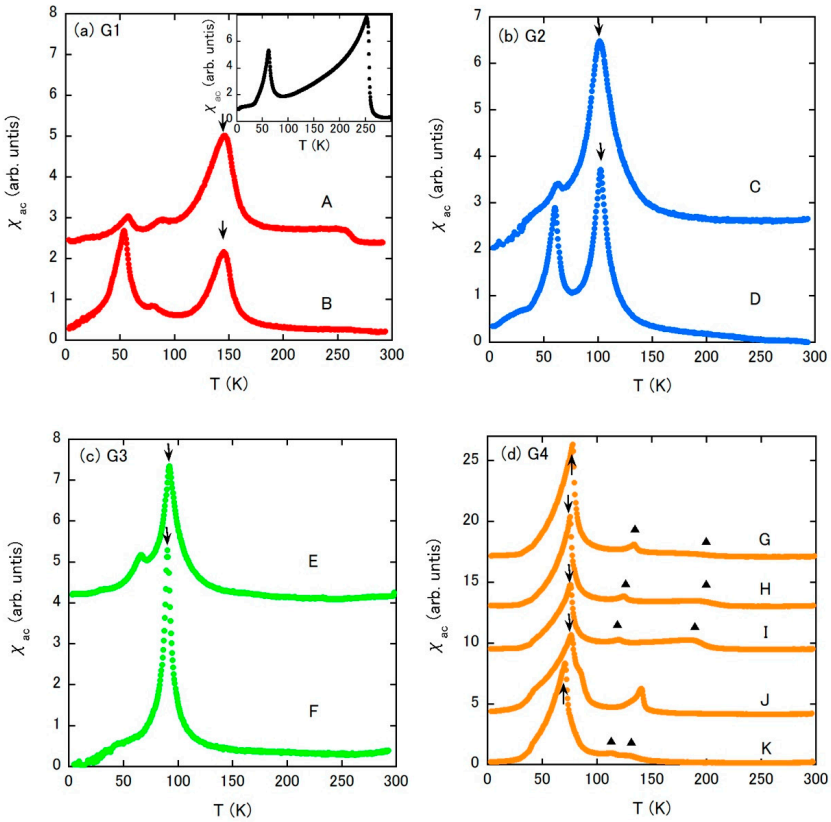

Figure 6. Temperature dependences of χ_{ac} for samples (**a**) A and B, (**b**) C and D, (**c**) E and F, and (**d**) G to K, respectively. The origin of each χ_{ac} is shifted by a value for clarity. The inset of (**a**) is the χ_{ac} (T) of the sample, with the starting composition of $Tb_{42.9}Co_{50}Ga_{7.1}$.

Figure 6d shows the χ_{ac} (T) of the G4 group. Except for sample J, two small anomalies due to impurity phases are observed, indicated by filled triangles in each sample. $Tb_{1-x}Co_xGa$ and $TbCo_{2-x}Ga_x$ are responsible for the low and high temperature anomalies, respectively. The value of x in $TbCo_{2-x}Ga_x$ is around 0.47 for each sample of G, H, and I, and 0.7 for sample K, respectively. The reduction trend of the magnetic transition temperature in $TbCo_{2-x}Ga_x$ with increasing x is in agreement with the results in the literature [12]. In sample J, the peak at approximately 140 K would be induced by $TbCo_{1-x}Ga_x$, and the χ_{ac} peak due to the Tb_2Co_2Ga phase is rather broad, reflecting the coexistence of two Tb_2Co_2Ga phases with slightly different atomic compositions. $Tb_{1-x}Co_xGa$ and $TbCo_{1-x}Ga_x$ may be related to TbGa with T_C = 154 K [14], which probably supports the assignment of magnetic impurity phases in Figure 6d. We remark that the shapes of the χ_{ac} peaks at T_C of the Tb_2Co_2Ga phases in the G4 group somewhat differ from those of the G1 to G3 groups. For the G4 group (Figure 6d), χ_{ac} shows a λ-type anomaly, and the χ_{ac} peaks of the G1 to G3 groups (Figure 6a–c) are more symmetric with respect to the temperature-axis.

Figure 7a shows χ_{dc} (T) under the external field of 10 Oe of samples A, C, F, and G, respectively. In each sample, χ_{dc} steeply increases below the approximate T_C of the Tb_2Co_2Ga phase. Figure 7b shows the temperature dependences of the inverse χ_{dc} of the four samples, which follow the Curie-Weiss law above 285 K, 275 K, 180 K, and 255 K, respectively (see the lines in Figure 7b). The effective magnetic moment μ_{eff} and the Weiss temperature Θ are summarized in Table 3. The value of μ_{eff} is near 9.72 μ_B/Tb, as expected for a free trivalent Tb ion, except in sample A, in which the narrow temperature range for the Curie–Weiss fitting may disturb an accurate extraction of μ_{eff}. From the χ_{dc} data, it is not clear whether the Co atom carries a magnetic moment or not.

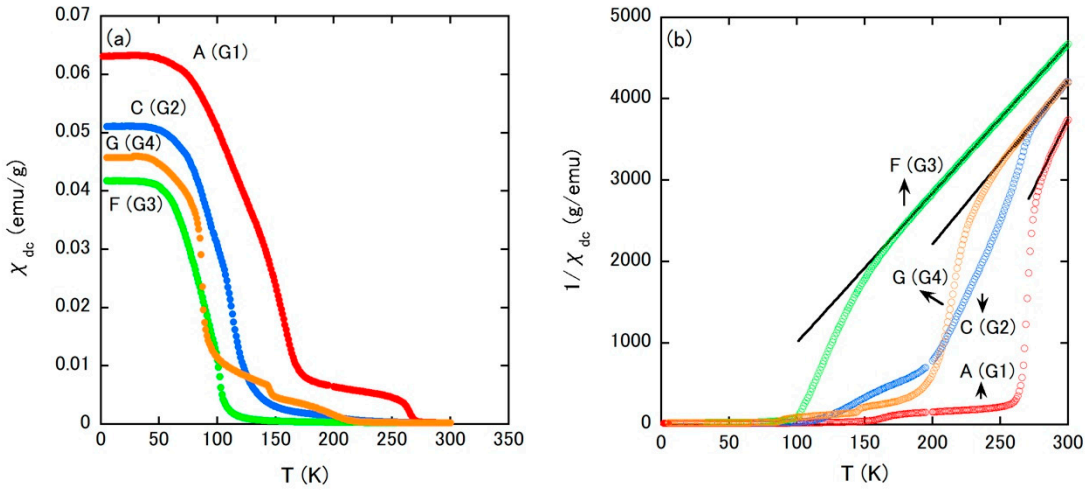

Figure 7. (**a**) Temperature dependences of χ_{dc} for samples A, C, F, and G. The external field is 10 Oe. (**b**) Temperature dependences of $1/\chi_{dc}$ for samples A, C, F, and G.

Figure 8a–d exhibit the *M*-*H* (*M*: magnetization and *H*: external field) curves measured at several temperatures denoted in the figures for samples A, C, F and G, respectively. In samples A, C, and F, below the T_C of the Tb_2Co_2Ga phases obvious hystereses grow, which are characteristic of ferromagnetism. For sample G in the G4 group, soft ferromagnetic behavior is observed down to 40 K, which might suggest that the ferromagnetic nature differs from those of samples A (G1), C (G2), and F (G3).

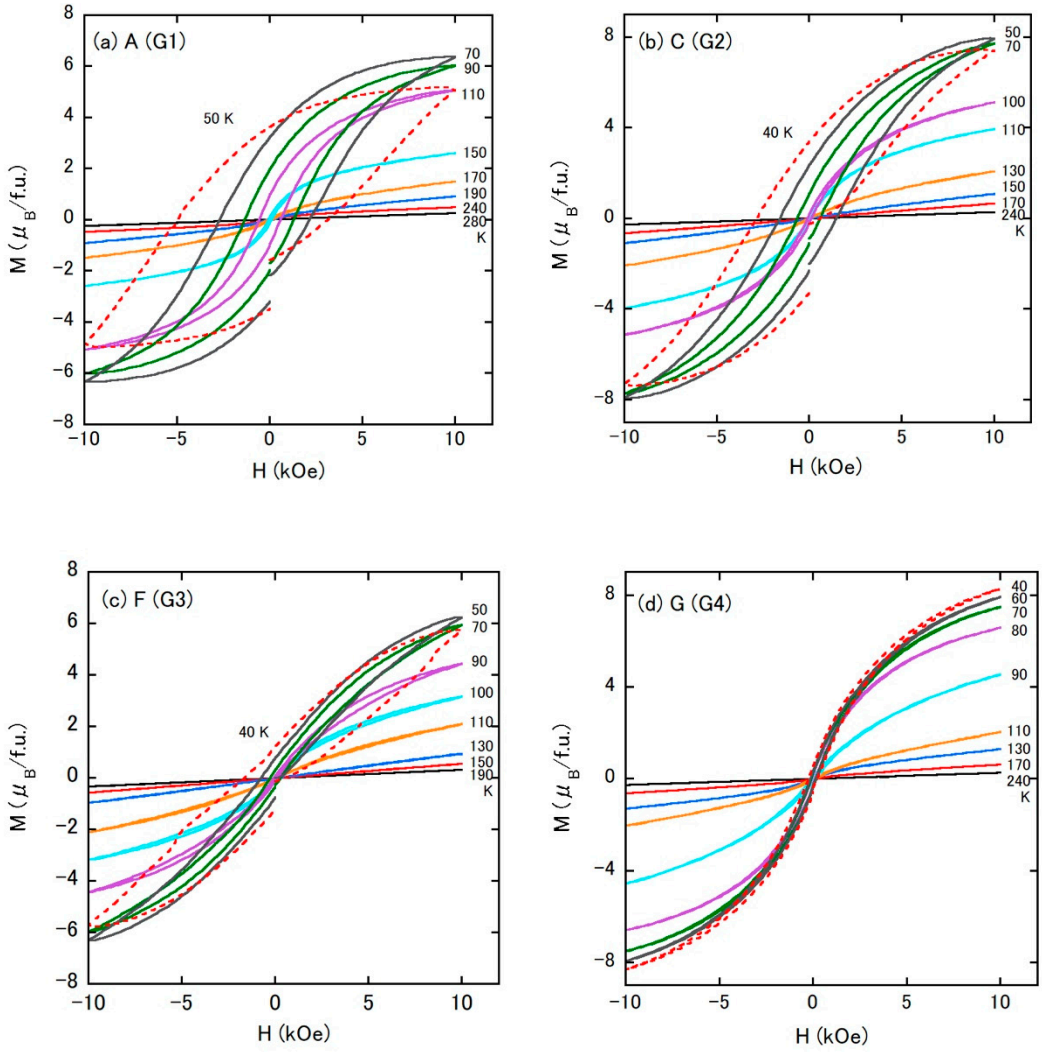

Figure 8. *M-H* curves measured at several temperatures as denoted in the figures for samples (**a**) A, (**b**) C, (**c**) F, and (**d**) G, respectively.

3.3. Relationship between the Ferromagnetic Properties and Crystal Structure Paremeters

Hereafter, we discuss the relationship between the crystal structure parameters and T_C. Figure 9a–c are the 3D bar graphs of T_C as a function of *a* and *b*, *a* and *c*, and *b* and *c*, respectively. In all figures, the G1 to G3 groups show systematic lattice parameter dependences of T_C; the increase of *a*(*b*) and the decrease of *c* reduce T_C. On the other hand, from the G3 to G4 group, the systematic dependence is not observed. All figures indicate that the samples in the G4 group can be divided into three subgroups of SG4-1, SG4-2, and SG4-3. Moreover, in the ternary phase diagram shown in Figure 2b, the starting atomic compositions of samples in the SG4-1 (SG4-3) subgroup are located in the region with a Tb concentration higher (lower) than that of sample I (SG4-2). As shown in Table 1, the order of the actual Tb compositions in the G4 group is consistent with that of the starting compositions, although the difference between the samples is smaller for the actual composition. Therefore, there might be some correlation between the lattice parameters and the Tb concentration for the G4 group. We note that the T_C of the sample in the G4 group seems to be slightly reduced with decreasing Tb concentration (see Table 3).

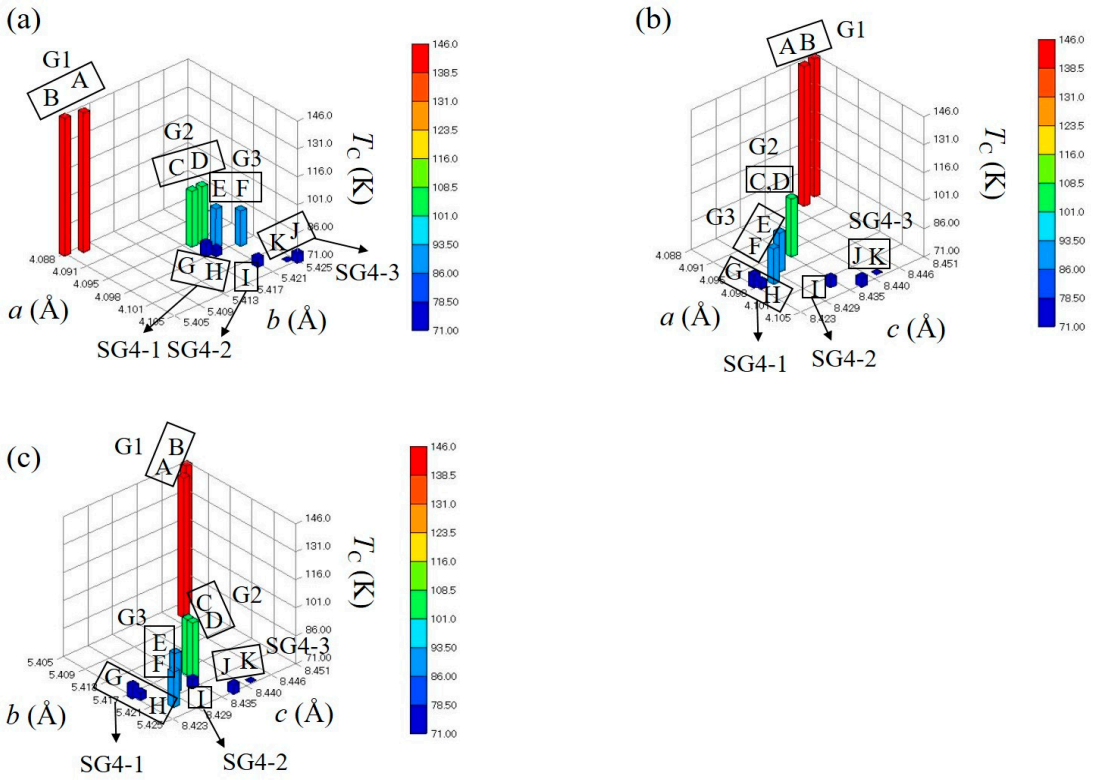

Figure 9. 3D bar graphs of T_C as a function of (**a**) a and b, (**b**) a and c, and (**c**) b and c, respectively.

Shown in Figure 10a,b are the 3D bar graphs of T_C as a function of Tb–Tb and Tb–Co, and θ_1 and θ_2, respectively, especially focusing on the octahedron formed by the Tb and Co atoms (see also Figure 1). The Tb–Tb (Tb–Co) means the nearest Tb–Tb (Tb–Co) distance, and θ_1 and θ_2 are Co–Tb–Co angles in the octahedron. From the G1 to G3 groups, as the nearest Tb–Tb (Tb–Co) distance monotonously decreases (increases), T_C is reduced from ~145 K to ~90 K. Then, both θ_1 and θ_2 become wider, and Figure 10a,b for the G1 to G3 groups suggest that the octahedron being compressed along the c-axis leads to the T_C reduction. The expansion of Tb–Co distance in particular means a weakened RKKY interaction through the weakened hybridization between the Tb and Co atoms. This might be responsible for the reduction of T_C down to 90 K. At the present stage, the origin of further reductions of T_C down to ~75 K is unclear; however, a possible change of ferromagnetic properties in the G4 group can be conjectured as below. From the G3 to the G4 group, θ_1 becomes narrower, while on the other hand, θ_2 apparently continues to increase. The anisotropic behavior of the octahedral parameters is related to the difference of shapes of the χ_{ac} peaks at T_C between the samples in the G1 to G3 groups and those in the G4 group, as mentioned above.

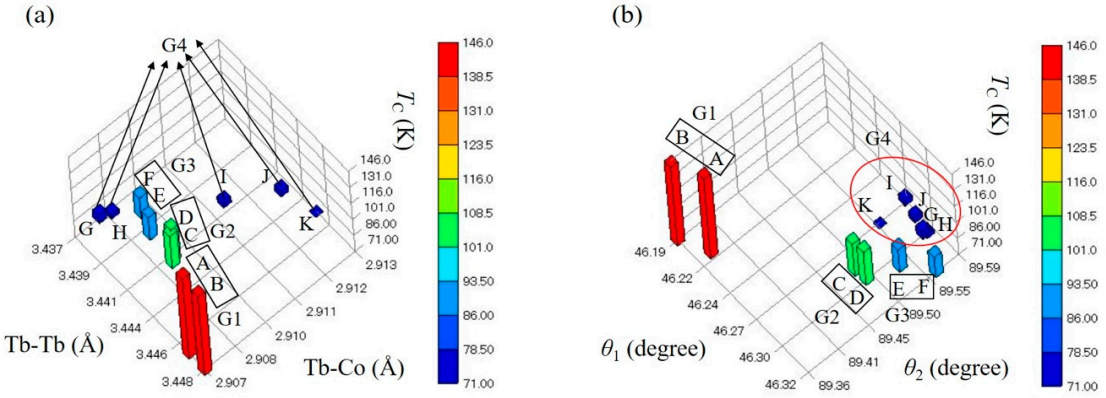

Figure 10. 3D bar graphs of T_C as a function of (**a**) Tb–Tb and Tb–Co, and (**b**) θ_1 and θ_2, respectively. The errors of Tb–Tb and Tb–Co distances are 0.0005 Å, 0.0003 Å, respectively. That of θ_1 and θ_2 is 0.007°.

4. Conclusions

The composition effect of the ferromagnetic properties in Tb_2Co_2Ga, crystallizing into an orthorhombic W_2CoB_2-type structure, was investigated. The atomic composition obtained by the EDX measurement revealed the existence of a homogeneity range. The compound shows a remarkable composition effect of T_C that is sensitive to the atomic composition, and ranges rather widely, i.e., from 75 to 145 K. The composition dependence of T_C is ascribed to the differences in the crystal structure parameters. For the samples in the G1 to G3 groups, the Tb–Tb and Tb–Co distances would be important factors in determining T_C. The decrease of the Tb–Tb distance leads to an increase of the Tb–Co distance, which weakens the RKKY interaction through weakened hybridization between the Tb and Co atoms. The samples in the G4 group can be divided into three subgroups by the lattice parameter dependences of T_C, but the θ_1 and θ_2 angles in each sample show similar values. The anisotropic change of two angles below a T_C of ~90 K makes the crystal feature of the octahedron different from that of the samples in the G1 to G3 groups. In reality, the anisotropic modification of the octahedron in the sample of the G4 group would be reflected in the λ-type χ_{ac} anomaly at T_C, which differs from those of the samples in the G1 to G3 groups.

Author Contributions: Conceptualization, J.K., N.S. and M.T.; methodology, J.K., N.S and M.T.; formal analysis, J.K. and M.T.; investigation, S.T., H.T. and N.S.; writing—original draft preparation, J.K.; writing—review and editing, J.K., N.S. and M.T.

Funding: This research received no external funding.

Acknowledgments: J.K. is grateful for the support provided by the Comprehensive Research Organization of Fukuoka Institute of Technology.

Conflicts of Interest: The authors declare no conflict of interest.

References

1. Rieger, W.; Nowotny, H.; Benesovsky, F. Die kristallstruktur von W_2CoB_2 und isotypen phasen. *Mon. Chem.* **1966**, *97*, 378–382. [CrossRef]
2. Sengupta, K.; Iyer, K.K.; Sampathkumaran, E.V. Large magnetoresistance and magnetocaloric effect above 70 K in Gd_2Co_2Al, Gd_2Co_2Ga, and Gd_7Rh_3. *Phys. Rev. B* **2005**, *72*, 054422. [CrossRef]
3. Fu, H.; Zou, M.; Guo, M.S.; Zheng, Q.; Zu, X.T. Structural, magnetic, and magnetothermal properties of R_2Co_2Al (R = Tb, and Dy) compounds. *Mater. Charact.* **2011**, *62*, 451–455. [CrossRef]
4. Morozkin, A.V.; Genchel, V.K.; Garchev, A.V.; Yapaskurt, V.O.; Isnard, O.; Yao, J.; Nirmala, R.; Quezado, S.; Malik, S.K. Magnetic ordering of Mo_2NiB_2-type $(Gd, Tb, Dy)_2Co_2Al$ compounds by magnetization and neutron diffraction study. *J. Magn. Magn. Mater.* **2017**, *442*, 36–44. [CrossRef]

5. Morozkin, A.V.; Garchev, A.V.; Yapaskurt, V.O.; Yao, J.; Nirmala, R.; Quezado, S.; Malik, S.K. Mo_2NiB_2-type Sm_2Co_2Al and Sm_2Co_2Ga compounds: Magnetic properties and giant low-temperature coercivity. *J. Solid State Chem.* **2018**, *260*, 95–100. [CrossRef]
6. Kitagawa, J.; Terada, H.; Shirakawa, N.; Tsubota, M.; Nose, A.; Tanaka, S. Composition effect in ferromagnetic properties of Tb_3Co_3Ga. *Res. Phys.* **2019**, *15*, 102591. [CrossRef]
7. Morozkin, A.V.; Yao, J.; Knotko, A.V.; Yapaskurt, V.O. Low-temperature coercivity of Mo_2NiB_2-type Tb_2Co_2Ga and Tb_2Co_2Al-based solid solutions. *J. Solid State Chem.* **2019**, *277*, 406–414. [CrossRef]
8. Kitagawa, J.; Takeda, N.; Sakai, F.; Ishikawa, M. Effect of composition in (RE) $_3$Pd $_{20}$Ge $_6$ (RE=La, Ce and Nd). *J. Phys. Soc. Jpn.* **1999**, *68*, 3413–3416. [CrossRef]
9. Lu, Q.M.; Yue, M.; Zhang, H.G.; Wang, M.L.; Yu, F.; Huang, Q.Z.; Ryan, D.H.; Altounian, Z. Intrinsic magnetic properties of single-phase Mn1+xGa ($0 < x < 1$) alloys. *Sci. Rep.* **2015**, *5*, 17086. [PubMed]
10. Izumi, F.; Momma, K. Three-dimensional visualization in powder diffraction. *Solid State Phenom.* **2007**, *130*, 15–20. [CrossRef]
11. Tsubota, M.; Kitagawa, J. A necessary criterion for obtaining accurate lattice parameters by Rietveld method. *Sci. Rep.* **2017**, *7*, 15381. [CrossRef] [PubMed]
12. Dębiec, I.; Chełkowska, G. Magnetic, electric and XPS study of $Tb(Co_{1-x}Ga_x)_2$ compounds. *J. Magn. Magn. Mater.* **2003**, *261*, 73–77. [CrossRef]
13. Miyahara, J.; Shirakawa, N.; Setoguchi, Y.; Tsubota, M.; Kuroiwa, K.; Kitagawa, J. Hill plot focusing on Ce compounds with high magnetic ordering temperatures and consequent study of Ce_2AuP_3. *J. Supercond. Nov. Magn.* **2018**, *31*, 3559–3564. [CrossRef]
14. Zheng, X.Q.; Chen, J.; Shen, J.; Zhang, H.; Xu, Z.Y.; Gao, W.W.; Wu, J.F.; Hu, F.X.; Sun, J.R.; Shen, B.G. Large refrigerant capacity of RGa (R = Tb and Dy) compounds. *J. Appl. Phys.* **2012**, *111*, 07A917. [CrossRef]